



Solid-state NMR measurement of Ψ in peptides: a NCCN 2Q-heteronuclear local field experiment

P.R. Costa, J.D. Gross, M. Hong, R.G. Griffin

Francis Bitter Magnet Laboratory and Department of Chemistry, MIT, Cambridge, MA 02139, USA

Received 3 June 1997; in final form 9 September 1997

Abstract

A solid-state NMR experiment is presented for measuring Ψ torsion angles in (^{15}N - $^{13}\text{C}_\alpha$ - $^{13}\text{C}_\beta$ - ^{15}N)-labeled peptides. Creation of $^{13}\text{C}_\alpha$ - $^{13}\text{C}_\beta$ double-quantum coherence (DQC) is followed by selective evolution under ^{15}N - ^{13}C dipolar interactions. The time-course of $^{13}\text{C}_\alpha$ - $^{13}\text{C}_\beta$ DQC dephasing is sensitive to the Ψ torsion angle, particularly for values associated with β -sheet secondary structure (120–180°). We apply the technique to glycylglycine · HCl and extract a value for Ψ that matches the diffraction-determined value ($\Psi = 162.1^\circ$) with a precision of $\pm 5^\circ$. © 1997 Published by Elsevier Science B.V.

1. Introduction

In recent years solid-state nuclear magnetic resonance (ssNMR) has proven crucial for investigating the structure of macroscopically disordered biological solids (including lyophilized [1] and membrane [2,3] proteins and peptide aggregates [4,5]). In these systems the details of molecular structure are inaccessible to the more traditional methods of investigation (i.e. X-ray crystallography and liquid-state NMR). The precision of structural models derived using ssNMR techniques does not yet approach the standard that has been set in other areas of structural biology. An intense effort continues to improve both the accuracy and range of the internuclear distance measuring techniques [6–8] which have formed the basis of many ssNMR structural investigations. But alternative experimental approaches which provide complementary data that can increase structural resolution are also of obvious interest.

Feng et al. [9], have recently proposed a novel, magic angle spinning (MAS)-based method for measuring torsion angles about ^{13}C - ^{13}C bonds (denoted 2Q-heteronuclear local field (HLF)) by examining the relative orientation of the two directly-bonded ^{13}C - ^1H dipolar interactions. A similar proposal has been made for ^{15}N - ^{13}C torsion angles [10]. These experiments are examples of a general class of measurements which correlate spatially anisotropic spin interactions such as the dipolar coupling and the chemical shift anisotropy (CSA) to extract structural information [11–19]. Because these techniques correlate large spin interactions, they are more easily extended to multiply labeled samples, whereas the weak internuclear dipolar interactions whose magnitudes provide useful distance information may be obscured by strong couplings between directly-bonded nuclei.

The HCCH 2Q-HLF experiment requires creation of ^{13}C - ^{13}C double-quantum coherence (DQC), fol-

lowed by a period of DQC dephasing driven solely by the ^{13}C - ^1H dipolar interactions. The use of DQC [17] as opposed to sequential periods of single-quantum dephasing [18,19] allows acquisition of a subset of the accessible tensor correlation information and the benefits of a single mixing period and double-quantum filtering. Subsequent evolution of the DQC driven by the ^{13}C - ^1H dipolar interactions is detected by constant-time division of a single rotor period, τ_r , into CW heteronuclear and MREV [20,21] homonuclear decoupling periods applied to the ^1H channel. During τ_r the DQC first dephases, and then rephases as the ^{13}C - ^1H coupling is refocused by MAS. The manner in which dephasing occurs depends on the relative orientation of the ^{13}C - ^1H dipolar tensors, and hence the CC torsion angle. The ease and accuracy with which this experiment allows measurement of certain structural parameters in spinning solids represents a significant technical advance. However the HCCH method, as currently constituted, does have several drawbacks which include the following. In these experiments the condition $\omega_r < \delta_d/3$ must be satisfied, where δ_d is the multiple-pulse scaled

^1H - ^{13}C dipolar coupling constant, to achieve significant dephasing (methods for increasing the effective coupling strength during the dephasing period have been devised [22]). Hence these experiments have typically been performed in the slow (3–4 kHz) spinning regime. Furthermore, the time resolution with which data is gathered is limited by the length of the MREV pulse cycle (or subcycle). These two requirements constitute significant limitations of the technique, particularly if extension to uniformly labeled samples is desired.

Here we describe a modification of the 2Q-HLF concept applied to a ^{15}N - ^{13}C - ^{13}C - ^{15}N (NCCN) spin quartet. Creation of $^{13}\text{C}_2$ DQC, followed by dephasing solely under the influence of the ^{15}N - ^{13}C heteronuclear couplings, will yield a DQC dephasing curve whose shape provides information about the relative orientation of the ^{15}N - ^{13}C couplings, and hence the ^{13}C - ^{13}C torsion angle. This corresponds to the Ψ angle along a peptide backbone when the ^{13}C nuclei are directly-bonded α - and carbonyl carbons (Fig. 1A). By recoupling the ^{15}N - ^{13}C interactions during the dephasing period, rather than observing

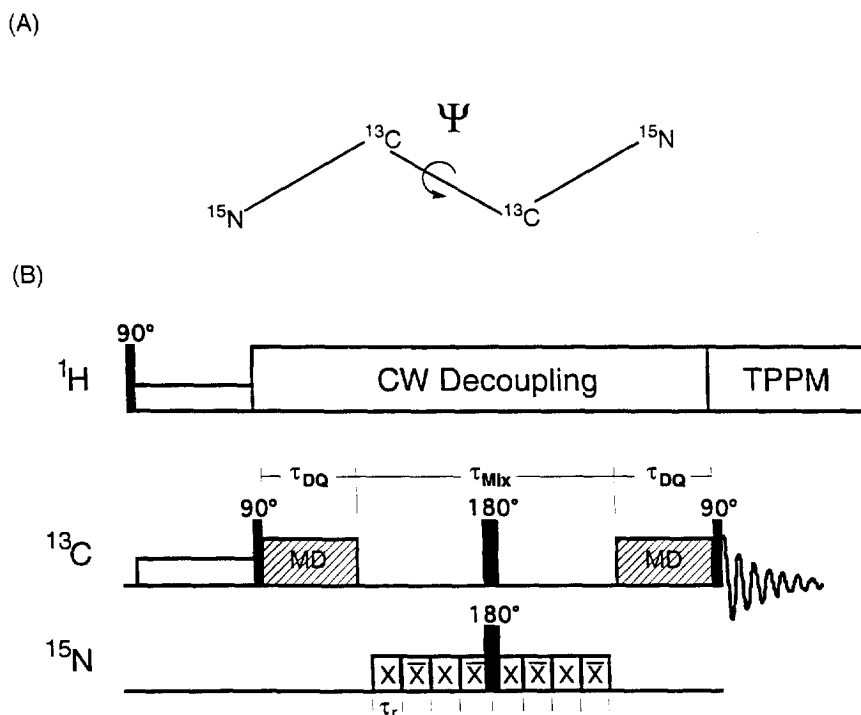


Fig. 1. (A) Isotope labeling scheme and (B) pulse sequence for NCCN 2Q-HLF Ψ torsion angle measurement.

their effects during a single rotor cycle at (very) slow spinning speed, we are able to perform the experiment effectively at much higher spinning speeds and with finer time resolution. The result is an experiment that, at least in certain torsion angle regimes, is exquisitely sensitive to conformation. Because the $^{13}\text{C}=\text{O}$ lacks a bound ^1H , this represents a unique approach (short of ^{17}O NMR) of applying the 2Q-HLF concept to measuring peptide backbone Ψ angles.

The selection of the appropriate pulse sequence elements for DQ filtering and ^{15}N – ^{13}C recoupling is flexible within this framework. The selections used in the implementation presented here (Fig. 1B) were guided by the desire for efficient operation at relatively high spinning speeds in uniformly (^{13}C , ^{15}N)-labeled molecules.

2. Pulse sequence and calculations

The pulse sequence is diagrammed in Fig. 1B, and includes the standard cross-polarization from ^1H to ^{13}C nuclei followed by CW decoupling on the ^1H channel during mixing and TPPM decoupling [23] during acquisition. We then use the MELODRAMA-4.5 [24] (MD) pulse sequence, which requires a rf magnitude 4.5 times the spinning speed, to create DQ coherence. Although other techniques have higher theoretical DQ filter efficiencies, they either require prohibitively high rf powers at high spinning speeds (e.g. C7 [25] requires $\omega_{\text{rf}} = 7 \times \omega_r$), or have their efficiency compromised by the relatively large chemical shift difference between α - and carbonyl carbons (e.g. 2Q-HORROR [26]), unless very high (> 20 kHz) spinning speeds can be achieved.

The creation of $^{13}\text{C}_2$ DQC from longitudinal sum polarization using the MD sequence is straightforward and has been described previously using Average Hamiltonian Theory [24]. The spin part of the recoupled dipolar interaction does not have a rotor phase dependence in the MD experiment, so that the form of the DQ component of the density operator is identical for all crystallites after the first DQ mixing period, and can be written:

$$\rho = C_{1X}C_{2X} - C_{1Y}C_{2Y}, \quad (1)$$

where C_1 and C_2 represent the spin operators for the two ^{13}C nuclei.

We apply ^{15}N rf to recouple the ^{13}C – ^{15}N dipolar interaction in the period following DQC creation. The ^{15}N rf magnitude is set to match the spinning speed ($\omega_{\text{rf}} = \omega_r$) as in the R^3 [27] experiment. The rf phase is inverted every rotor cycle (analogous to SPICP [28]). R^3 -related techniques allow for recoupling with low rf power even at high spinning speeds without the finite pulse effects associated with pulsed recoupling techniques which increase as the rotor period shrinks. The absence of rf power on the ^{13}C channel, where a strong homonuclear dipolar interaction is present, is also beneficial. Phase inversion has several effects including (i) removal of the ^{15}N CSA dependence of dipolar dynamics induced by unmodified R^3 ; (ii) compensation for ^{15}N isotropic shift offsets and rf inhomogeneity (demonstrated below). We term the combined technique synchronous phase inversion rotary resonance recoupling (SPI- R^3). Note that 180° pulses in the center of the dephasing period on both ^{13}C and ^{15}N channels refocus ^{13}C chemical shifts while preserving the recoupled dipolar interaction.

The SPI- R^3 -induced recoupling effect is illustrated by calculation of the zeroth-order average Hamiltonian for the sequence in the appropriate interaction frame. Given the rotating-frame Hamiltonian for a ^{13}C , ^{15}N spin pair (represented by C and N operators):

$$H = n\omega_r N_X + \omega_D^{\text{CN}}(t)2C_Z N_Z \quad (2)$$

(where we have assumed on-resonance irradiation of the ^{15}N nucleus with rf magnitude equal to a multiple n of the spinning speed), transformation to the interaction frame defined by the rf term yields:

$$\begin{aligned} \bar{H} = C_Z \sum_{\substack{m=-2 \\ (m \neq 0)}}^2 & (\omega_D^{\text{CN}(m)} N_+ e^{i(n+m)\omega_r t} \\ & + \omega_D^{\text{CN}(-m)} N_- e^{-i(n-m)\omega_r t}), \end{aligned} \quad (3)$$

where the time-dependence imposed on the coupling by MAS

$$\omega_D^{\text{CN}}(t) = \sum_{\substack{m=-2 \\ m \neq 0}}^2 \omega_D^{\text{CN}(m)} e^{im\omega_r t} \quad (4)$$

has been explicitly included, and the raising and lowering operators are defined relative to X as the quantization axis). Subsequent averaging over one

rotor cycle yields the zero-order average Hamiltonian for the basic R³ experiment:

$$\begin{aligned} \bar{H}^{(0)} = C_Z \sum_{\substack{m=-2 \\ (m \neq 0)}}^2 & (\omega_D^{\text{CN}(m)} N_+ \delta_{n,-m} \\ & + \omega_D^{\text{CN}(-m)} N_- \delta_{n,m}), \end{aligned} \quad (5)$$

which for $n = 1$ simplifies to:

$$\begin{aligned} \bar{H}^{(0)} = C_Z & (\omega_D^{\text{CN}(-1)} N_+ + \omega_D^{\text{CN}(1)} N_-) \\ = |\omega_D^{\text{CN}(1)}| C_Z & (N_Z \cos \gamma_D^{\text{CN}} + N_Y \sin \gamma_D^{\text{CN}}), \end{aligned} \quad (6)$$

where γ_D^{CN} represents the phase of the CN dipolar axis about the rotor axis. Note that the ¹⁵N CSA is similarly recoupled under these conditions — the calculation of the effect proceeds along identical lines but with C_Z dropped. If the ¹⁵N CSA and ¹⁵N–¹³C dipolar interactions have different rotor phase angles, their recoupled spin components (evident in Eq. (6)) will not commute. This results in ¹³C-detected dipolar dephasing dynamics that depend upon both the size and orientation of the ¹⁵N CSA relative to the heteronuclear dipolar axis.

Rotor-synchronized phase inversions remove the ¹⁵N CSA dependence of ¹³C-detected dephasing dynamics. The average Hamiltonian for the second rotor cycle in the sequence is derived from (5) by inverting the sign of n , yielding (as the equivalent of Eq. (6)):

$$\begin{aligned} \bar{H}^{(0)} = C_Z & (\omega_D^{\text{CN}(1)} N_+ + \omega_D^{\text{CN}(-1)} N_-) \\ = |\omega_D^{\text{CN}(1)}| C_Z & (N_Z \cos \gamma_D^{\text{CN}} - N_Y \sin \gamma_D^{\text{CN}}). \end{aligned} \quad (7)$$

The zero-order average Hamiltonian for the entire SPI-R³ sequence can be derived by simply adding the averages for successive rotor cycles:

$$\bar{H}^{(0)} = |\omega_D^{\text{CN}(1)}| C_Z N_Z \cos \gamma_D^{\text{CN}}. \quad (8)$$

The recoupled ¹⁵N CSA has a similar dependence on N_Z . Hence commutation between the two is achieved at the expense of γ_D -dependent recoupled dipolar magnitudes. Simulations (not shown) indicate that γ -dependent ¹⁵N–¹³C recoupling does not strongly affect the ability to measure torsion angles using DQ dephasing curves, described below.

The rf inhomogeneity compensation of the rotor-synchronized phase inversion follows from a similar

cancellation: a positive offset from resonance ($\omega_{\text{rf}} = \omega_r + \delta\omega$) during one rotor cycle becomes a negative offset during the next ($\omega_{\text{rf}} = -\omega_r - \delta\omega$), so that summing over successive rotor cycles cancels any residual rf component that remains after averaging the nearest-resonant-frame transformed Hamiltonian (of Eq. (6)) over a single rotor cycle. Isotropic chemical shift offsets are compensated in a similar manner, as long as the length of each single-phase rf pulse is equivalent to an integer multiple of a 360° rotation. Both compensation effects depend on the fact that the rate at which phase inversion cycles occur ($\omega_r/2$) is much larger than the resonance offset ($\delta\omega$). We demonstrate experimentally below that typical offset and rf inhomogeneity values have no discernible effect on SPI-R³-induced ¹⁵N–¹³C dephasing dynamics.

In a 4-spin N₁–C₁–C₂–N₂ system, the directly-bonded N–C dipolar interactions drive the evolution of ¹³C₂ DQ coherence (from Eq. (1)) according to:

$$\begin{aligned} \rho = & (C_{1X} \cos b_1 \tau_{\text{MIX}} + C_{1Y} N_{1Z} \sin b_1 \tau_{\text{MIX}}) \\ & \times (C_{2X} \cos b_2 \tau_{\text{MIX}} + C_{2Y} N_{2Z} \sin b_2 \tau_{\text{MIX}}) \\ & - (C_{1Y} \cos b_1 \tau_{\text{MIX}} - C_{1X} N_{1Z} \sin b_1 \tau_{\text{MIX}}) \\ & \times (C_{2Y} \cos b_2 \tau_{\text{MIX}} - C_{2X} C_{2Z} \sin b_2 \tau_{\text{MIX}}), \end{aligned} \quad (9)$$

where b_1 and b_2 represent the magnitudes of the recoupled interactions and are implicitly orientation dependent. The DQ filtering process completed by the second MD step (phase cycled relative to the first MD period and the receiver phase appropriately [29]) converts only the components of the density matrix that have the form of Eq. (1) back to detectable signal, so that the time-dependence of our effective observable during the dephasing period is:

$$\begin{aligned} \langle O \rangle_{\tau_{\text{MIX}}} = & \langle C_{1X} C_{2X} - C_{1Y} C_{2Y} \rangle_{\tau_{\text{MIX}}} \\ = & \frac{1}{2} [\cos(b_1 \tau_{\text{MIX}} + b_2 \tau_{\text{MIX}}) \\ & + \cos(b_1 \tau_{\text{MIX}} - b_2 \tau_{\text{MIX}})]. \end{aligned} \quad (10)$$

Calculation of the observed signal as a function of the torsion angle Ψ requires averaging Eq. (10) over an isotropic distribution of molecular orientations, with b_1 and b_2 determined in each case by the overall molecular orientation and the peptide backbone geometry. Fig. 2A displays the standard backbone geometry, and Fig. 2B shows the DQ dephas-

ing curves calculated based on that geometry, with Ψ varying from 0° to 180° in 20° increments. The calculations in this case (based on numerical integration of the equations of motion derived from the rotating frame Hamiltonian rather than Eq. (10)) include only the dephasing effects of the directly-bonded N–C couplings. Although the strength and relative orientation of the longer-range N–C couplings are also fixed by Ψ and hence easily included

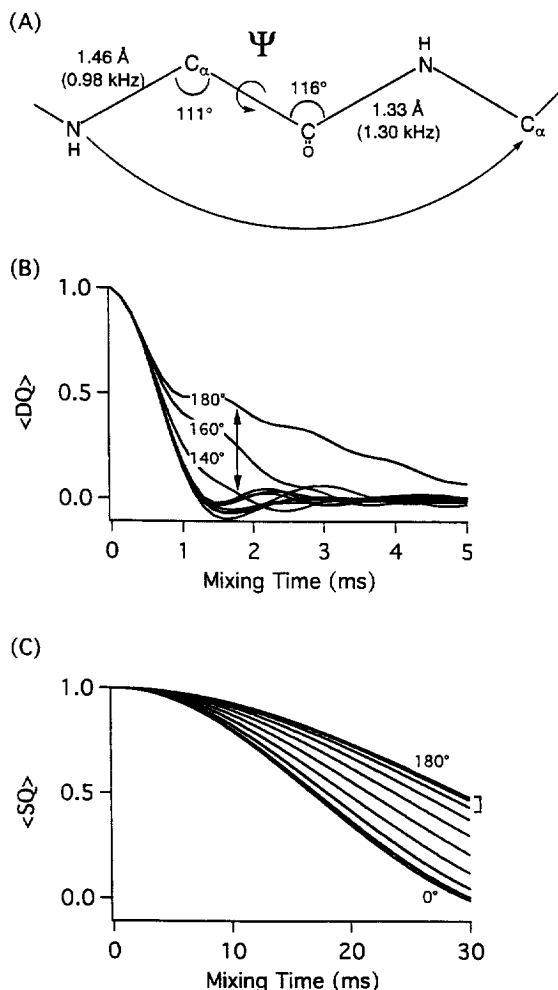


Fig. 2. Simulated dephasing curves as a function of the NCCN torsion angle Ψ . (A) diagrams the relevant peptide backbone geometry. (B) shows the calculated dephasing of double-quantum coherence during mixing as a function of Ψ (curves for Ψ varying from 0° to 180° in 20° increments are displayed). For comparison, (C) displays the calculated REDOR curves (single-quantum dephasing) for the N–C α internuclear distance indicated in (A) as a function of Ψ (again in 20° increments).

in calculations, their effect is minimal (shown below), and we do not include them here.

Note that simulations for (Ψ, Ψ') values related by the relation $\Psi = 360^\circ - \Psi'$ are identical. In other words, conformations which are equidistant from either cis or trans configurations (i.e. eclipsed or fully staggered N-to-N orientations, respectively) in the opposite rotational sense about the C–C bond will yield identical simulations. An identical symmetry holds true for the HCCH and related techniques. If the cis and trans symmetry conformations lie in the center of a highly populated conformational region, structural resolution will be reduced because of the inability to distinguish between conformations on either side of the symmetry. One useful benefit of the NCCN technique is that the symmetry conformations ($\Psi = 0^\circ$ and 180°) do not lie near the center of such populated regions.

The DQ dephasing curves are particularly sensitive to variations in Ψ near the trans regime (120° – 180°). When $\Psi = 180^\circ$ the two NC dipolar couplings are most closely aligned, so are recoupled with near identical efficiency for all molecular orientations. Assuming similar coupling constants, this implies that b_1 and b_2 of Eq. (10) will be similar for all molecular orientations, and hence that half of the detected signal will decay at a relatively slow rate determined by $(b_1 - b_2)$ averaged across the powder. This ‘‘cancellation’’ effect has been described by Levitt and co-workers [9]. As Ψ deviates from 180° , the recoupling efficiencies begin to differ widely, and both parts of Eq. (10) describe a fast decay.

It is during the transition between these two regimes that the dephasing curves are most sensitive to Ψ – in fact exquisitely so. We can compare them, for example, to a N–C α REDOR [30] distance measurement. As Ψ varies from 180° to 140° , this internuclear distance varies by $< 0.1 \text{ \AA}$, corresponding to the spread in single-quantum REDOR dephasing curves indicated by the bracket in Fig. 2C. The sensitivity of the two techniques to Ψ in this regime differs by an order of magnitude.

3. Results and discussion

Experimental results illustrating the effectiveness of the SPI-R³ heteronuclear dipolar dephasing se-

quence in two-spin ^{13}C – ^{15}N systems are displayed in Fig. 3. The sequence used in these experiments corresponds to that shown in Fig. 1 with the 90° pulses and MD evolution periods removed. The spinning speed was set to 14 kHz, and the matching ^{15}N rf field strength was determined using 2D nutation experiments. Applied to a polycrystalline glycine sample in which 10% of the molecules have a (^{15}N , $^{13}\text{C}_\alpha$) labeling scheme (obtained from Cambridge Isotope Labs, Cambridge, MA), the technique yields the SQ dephasing curve displayed in Fig. 3A.

The dashed line shows the decay of ^{13}C polarization in the absence of ^{15}N power; the dephasing data (filled circles) has been corrected for this decay as in a typical REDOR experiment [30]. Numerical simulations using a 0.9 kHz coupling constant (solid line) fit the data without the need to include the effects of rf inhomogeneity (measured to be $\approx 7\%$ FWHM), or ^{15}N CSA.

The phase-inversion compensation for ^{15}N offset and rf inhomogeneity is demonstrated in Fig. 3B and C. In Fig. 3B a series of experimental curves are

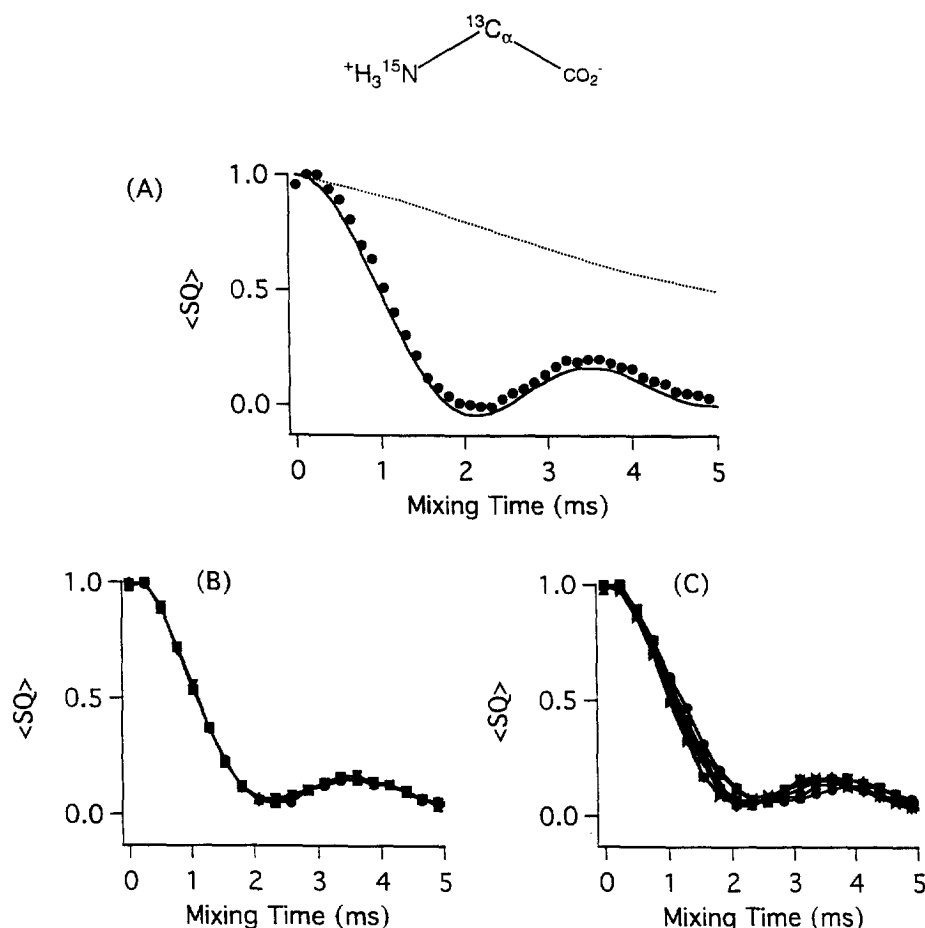


Fig. 3. Experimental demonstration of the SPI-R³ heteronuclear dipolar recoupling sequence on ^{15}N , $^{13}\text{C}_\alpha$ -labeled glycine (diluted 1:10 in natural abundance). (A) displays the single-quantum dephasing curve (filled circles) with $\omega_1 = 14$ kHz rf applied to ^{15}N and ^{13}C detection. The solid line shows the best-fit simulation ($b_{\text{IS}} = 0.90$ kHz; no correction for rf-inhomogeneity is necessary). The dotted line shows the measured decay of $^{13}\text{C}_\alpha$ polarization in the absence of ^{15}N rf (i.e. homogeneous relaxation); the dephasing data (filled circles) is corrected for this decay. (B) displays a series of dephasing curves obtained under identical conditions except for variation of the ^{15}N carrier frequency up to 3 kHz off-resonance. (C) displays a series of curves obtained with ^{15}N rf field strength varying up to 1.5 kHz away from the resonance value (14 kHz). Given the width of the rf nutation frequency distribution in our coil ($\approx 7\%$ FWHM), rf inhomogeneity is expected to have a negligible effect on the dephasing dynamics.

displayed in which the ^{15}N offset was increased from 0 to 3 kHz, and almost no detectable variation in the dephasing curves occurs. In Fig. 3C, the ^{15}N rf field strength was varied over a 3 kHz range spanning the resonance field strength (14 kHz); small variations do occur. Over a range corresponding to the measured rf inhomogeneity (≈ 1 kHz at this field strength) the variation is minimal.

$(^{15}\text{N}, ^{13}\text{C}_2)$ -glycyl- (^{15}N) -glycine \cdot HCl provides an appropriate sample to test the full NCCN DQ dephasing torsion angle experiment [31]. The relevant molecular geometry derived from a neutron diffraction study [32] is shown in Fig. 4A. In Fig. 4B we display the measured DQ dephasing curve (filled circles), which has been corrected for DQ decay without ^{15}N rf (open circles). The spinning speed was 14 kHz and the ^1H decoupling power throughout the experiment was 100 kHz. We obtained a DQ filtering efficiency of 20–25% with $\tau_{\text{DQ}} = 8\tau_r$, about half of the maximal efficiency obtainable with MD.

Calculation of the DQ dephasing curve based on the geometry of Fig. 4A and including all relevant interactions (long and short range NC, CC and NN dipolar couplings, estimated NC and CC J-couplings, and ^{15}N and ^{13}C CSA tensors [33]) matches the data quite well (lower solid line in Fig. 4B). The fluctuations in the data are primarily due to the low S/N obtained from the sample, which contained the labeled material diluted 1:40 in natural abundance material (hence the experiment is roughly equivalent to a measurement in a ca. 40–50 residue peptide). No natural abundance background subtraction is necessary in these experiments, as has been noted, due to the DQ filtering process. The measurement constrains the torsion angle to a relatively small range: simulations where Ψ is varied $\pm 5^\circ$ from the diffraction-determined value essentially bracket all of the data. This is a conservative estimate of the experimental precision.

The accuracy of measurements of this type will also depend on the sensitivity of the DQ dephasing curves to variations in molecular geometry other than that described by Ψ , and to other spin interactions. The calculated curves in Fig. 4C examine this issue. The thick line duplicates the $\Psi = 162.1^\circ$ curve from Fig. 4B, which includes the effects of long- and short-range dipolar and J-interactions and CSA tensors. The dotted line shows the calculation using

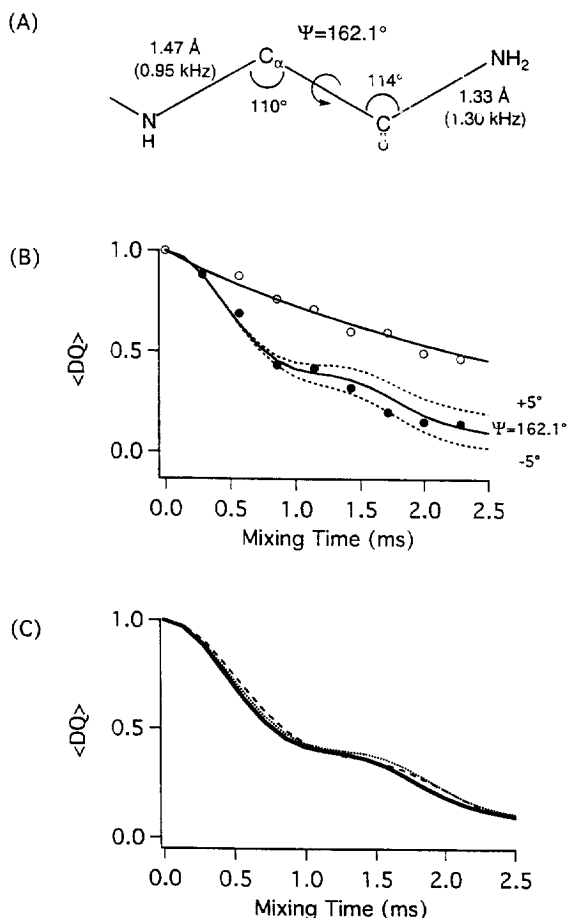


Fig. 4. Extraction of the NCCN (Ψ) torsion angle in glycyglycine \cdot HCl (diluted 1:40 in natural abundance). (A) displays the relevant molecular geometry. (B) displays the measured DQ dephasing, both with $\omega_1 = 14$ kHz ^{15}N rf power (filled circles), and without (open circles). Calculated dephasing curves with $\Psi = 162.1^\circ$ and $\pm 5^\circ$ are also displayed. (C) shows (i) the $\Psi = 162.1^\circ$ simulation from (B) (thick line), along with simulations in which (ii) C–C, N–N, and longer-range N–C couplings, all chemical shift and J-coupling terms have been ignored (dotted line); and (iii) similar to (ii) but with the generic backbone geometry of Fig. 2A (dashed line).

identical geometric parameters, but with all interactions except the directly-bonded N–C couplings ignored. Even though these interactions are relatively well-fixed by the local geometry as defined by Ψ and the bond lengths and angles, their presence clearly can be ignored to simplify the calculations. The dashed line includes this simplification, and also replaces the geometry of Fig. 4A which is specific to

the GG·HCl crystal structure with that for a “standard” peptide [34], shown in Fig. 2A. Again, little variation is seen. The overall range of variation corresponds to less than a 5° change in Ψ .

4. Conclusions

We have provided a general framework for measuring the peptide backbone torsion angle Ψ in solids that involves ^{13}C – ^{15}N dipolar dephasing of $^{13}\text{C}_\alpha$ – $^{13}\text{C}_=O$ DQ coherence. The specific implementation described here is designed to function effectively at relatively high spinning speeds. To that end we have proposed the SPI-R³ sequence to induce ^{15}N – ^{13}C dipolar dephasing without the necessity of applying high ^{15}N or ^{13}C rf power or the drawbacks associated with finite pulse effects and sensitivity to rf inhomogeneity. The efficiency of the DQ filtering component of the experiment is limited by the use of the MD sequence, but at high spinning speeds this is the best of few viable options. At slower speeds, the C7 sequence may be substituted for higher efficiency. The SPI-R³ sequence remains a competitive technique for inducing dipolar dephasing even at slow spinning speeds, but could conceivably be replaced by one of several alternatives including REDOR.

The region of high sensitivity to conformation ($\Psi = 120$ – 180°) corresponds roughly to the β -sheet structural regime. The extended nature of this type of secondary structure has made it difficult to accurately define the structural details of peptides in which it occurs [4,5] using distance measuring techniques with outer ranges of 5–6 Å. Application of the NCCN 2Q-HLF technique to these systems should be particularly useful in delineating the precise nature of their β -sheet conformation.

During the course of this work we learned that similar experiments were being performed by M. Levitt and co-workers [35].

Acknowledgements

This research was supported by the National Institutes of Health (GM-23403, NS-, and GM-23289, and RR-00995). Thanks are accorded to C.M. Rien-

stra for design and construction of transmission line probes used in this work.

References

- [1] L.M. McDowell, C.A. Klug, D.D. Beusen, J. Schaefer, *Biochemistry* 35 (1996) 5395.
- [2] A.E. McDermott, F. Creuzet, R. Gebhard, K. van der Hoef, M.H. Levitt, J. Herzfeld, J. Lugtenberg, R.G. Griffin, *Biochemistry* 33 (1994) 6129.
- [3] Y. Tomita, E.J. O'Connor, A. McDermott, *J. Am. Chem. Soc.* 116 (1994) 8766.
- [4] P.T.J. Lansbury, P.R. Costa, J.M. Griffiths, E.J. Simon, M. Auger, K.J. Halverson, D.A. Kocisko, Z.S. Hensch, T.T. Ashburn, R.G.S. Spencer, B. Tidor, R.G. Griffin, *Nature Struct. Biol.* 2 (1995) 990.
- [5] J. Heller, A.C. Kolbert, R. Larsen, M. Ernst, T. Bekker, M. Baldwin, S.B. Prusiner, A. Pines, D.E. Wemmer, *Protein Sci.* 5 (1996) 1655.
- [6] A.E. Bennett, C.M. Rienstra, P.T. Lansbury Jr., R.G. Griffin, *J. Chem. Phys.* 105 (1996) 10289.
- [7] M.A. Mehta, D.M. Gregory, S. Kiihne, D.J. Mitchell, M.E. Hatcher, J.C. Shiels, G.P. Drobny, *Solid State Nucl. Magn. Reson.* 7 (1996) 211.
- [8] P.R. Costa, B.Q. Sun, R.G. Griffin, *J. Am. Chem. Soc.*, in press.
- [9] X. Feng, Y.K. Lee, D. Sandstrom, M. Eden, H. Maisel, A. Sebald, M.H. Levitt, *Chem. Phys. Lett.* 257 (1996) 314.
- [10] M. Hong, J.D. Gross, R.G. Griffin, *J. Phys. Chem.* 101 (1997) 5869.
- [11] R.K. Hester, J.L. Ackermann, B.L. Neff, J.S. Waugh, *Phys. Rev. Lett.* 36 (1976) 1081.
- [12] M.E. Stoll, A.J. Vega, R.W. Vaughan, *J. Chem. Phys.* 65 (1976) 4093.
- [13] M. Linder, A. Hohener, R.R. Ernst, *J. Chem. Phys.* 73 (1980) 4959.
- [14] M.G. Munowitz, R.G. Griffin, *J. Chem. Phys.* 76 (1982) 2848.
- [15] P. Robyr, M. Tomaselli, J. Straka, C. Grob-Pisano, U.W. Suter, B.H. Meier, R.R. Ernst, *Mol. Phys.* 84 (1995) 995.
- [16] D.P. Weliky, R. Tycko, *J. Am. Chem. Soc.* 118 (1996) 8487.
- [17] K. Schmidt-Rohr, *J. Am. Chem. Soc.* 118 (1996) 7601.
- [18] Y. Ishii, T. Terao, M. Kainosho, *Chem. Phys. Lett.* 256 (1996) 133.
- [19] T. Fujiwara, T. Shimomura, H. Akutsu, *J. Magn. Reson.* 124 (1997) 147.
- [20] P. Mansfield, *J. Phys. C* 4 (1971) 1444.
- [21] W.-K. Rhim, D.D. Elleman, R.W. Vaughn, *J. Chem. Phys.* 59 (1973) 3740.
- [22] M. Hong, J.D. Gross, C.M. Rienstra, R.G. Griffin, K.K. Kumashiro, K. Schmidt-Rohr, *J. Magn. Reson.*, in press.
- [23] A.E. Bennett, C.M. Rienstra, M. Auger, K.V. Lakshmi, R.G. Griffin, *J. Chem. Phys.* 103 (1995) 6951.
- [24] B.-Q. Sun, P.R. Costa, D. Kocisko, P.T.J. Lansbury, R.G. Griffin, *J. Chem. Phys.* 102 (1995) 702.

- [25] Y.K. Lee, N.D. Kurur, M. Helmle, O.G. Johannessen, N.C. Nielsen, M.H. Levitt, *Chem. Phys. Lett.* 242 (1995) 304.
- [26] N.C. Nielsen, H. Bildsoe, H.J. Jakobsen, M.H. Levitt, *J. Chem. Phys.* 101 (1994) 1805.
- [27] T.G. Oas, R.G. Griffin, M.H. Levitt, *J. Chem. Phys.* 89 (1988) 692.
- [28] X. Wu, K.W. Zilm, *J. Magn. Reson. A* 104 (1993) 154.
- [29] R.R. Ernst, G. Bodenhausen, A. Wokaun, *Principles of Nuclear Magnetic Resonance in One and Two Dimensions*, Oxford University Press, Oxford, 1987.
- [30] T. Gullion, J. Schaefer, *J. Magn. Reson.* 81 (1989) 196.
- [31] (^{15}N)glycyl-($^{15}\text{N},^{13}\text{C}_2$)glycine · HCl was synthesized on Wang resin using standard Fmoc techniques. The peptide was purified by RPHPLC and diluted 1:40 in natural abundance glycylglycine · HCl in aqueous solution. Lyophilization yielded the final product.
- [32] T.F. Koetzle, W. Hamilton, *Acta Cryst. B* 28 (1972) 2083.
- [33] R.E. Stark, L.W. Jelinski, D.J. Ruben, D.A. Torchia, R.G. Griffin, *J. Magn. Reson.* 55 (1983) 266.
- [34] D. Voet, J.G. Voet, *Biochemistry*, John Wiley, New York, 1990.
- [35] X. Feng, M. Eden, A. Brinkmann, H. Luthman, L. Eriksson, A. Gresslund, O.N. Antzugin, M.H. Levitt, *J. Am. Chem. Soc.* (1997), in press.